PCCP

PAPER

View Article Online
View Journal

Cite this: DOI: 10.1039/c4cp04783d

Photoresponsive ionic liquid crystals based on azobenzene guanidinium salts†

Eugen Wuckert,‡[a] Marc D. Harjung,‡[b] Nadia Kapernaum,[b] Carsten Mueller,[b] Wolfgang Frey,[a] Angelika Baro,[a] Frank Giesselmann*[b] and Sabine Laschat*[a]

Received 20th October 2014,
Accepted 17th December 2014

DOI: 10.1039/c4cp04783d

www.rsc.org/pccp

The use of non-ionic LC phases as anisotropic matrices for *E*/*Z*-isomerization of azo-guest molecules is often restricted due to limited solubilities and demixing effects. In this study we therefore employed an ionic liquid crystal (ILC) matrix to follow the photo-induced *E*/*Z*-isomerization of ionic mesogenic azobenzene guanidinium guests. The latter were prepared from 4-hydroxy-4′-(octyloxy)azobenzene, which was first treated with *N*-(bromoalkyl)phthalimides to introduce the spacer with varying chain length. Removal of phthalimide and final reaction with a formamidinium salt linked the ionic head group to the photoisomerizable azobenzene unit. Investigation of the mesomorphic behaviour revealed for all azobenzene ILCs smectic A mesophases with high translational order parameters and partial bilayers, as could be stated by layer spacing *d*. Similar packing behaviour was found for the solid state by X-ray crystal structure analysis. *E*/*Z*-isomerization of azobenzene ILCs which were completely miscible with the ionic LC phase of C_{12}MIM-Br as anisotropic host was induced by irradiation with UV light and the reisomerization observed by time-resolved UV-Vis spectroscopy. For comparison, water was used as isotropic host. *Z*/*E*-reisomerization activation energies exhibited similar values of 97–100 kJ mol^{-1} irrespective of spacer lengths and the type of host. The results demonstrate that a proper match of steric requirements of host and guest as well as layer spacings are needed for a decreased activation energy.

1 Introduction

In the late seventies Pelzl[1] and Nelson[2] independently reported that the mesomorphic properties of azobenzenes and stilbenes can be changed by *E*/*Z*-photoisomerization. Later work by Ikeda showed that photochromic azobenzene guests in a nematic 5CB (4′-pentyl-cyanobiphenyl) host can induce photochemical isothermal phase transitions of the guest–host mixture.[3] These seminal contributions stimulated numerous research activities on the photoisomerization of thermotropic low molecular weight liquid crystals[4] as well as liquid crystalline polymers.[5] In contrast, only a few examples of ionic liquid crystals (ILCs) bearing mesogenic azobenzene units have been described up to now.[6] Chen prepared vinylimidazolium ILCs with *p*-nitroazobenzene[7] and symmetric azobenzenes with two imidazolium ions.[8] Kaszynski studied ILCs based on [*closo*-1-CB_9H_{10}]$^-$ clusters, where the *closo*-monocarborate is part of an "azo-heterobenzene" unit.[9] More recently, Deng reported the photo-induced isothermal phase transition of *N*-dodecyl-*N*-methyl-imidazolium tetrafluoroborate doped with small amounts of 4-methoxy-4′-methylazobenzene.[10] In such ILCs nanosegregation of charged head groups and lipophilic side chains and/or aromatic mesogenic subunits in combination with steric constraints is the major driving force for the formation of mesophases,[11] resulting in novel materials with fluid-like viscosity, long-range orientational order and anisotropic physical properties. Thus, ILCs may be considered as anisotropically ordered fluids.

Non-ionic liquid crystalline phases were used as anisotropic matrices in which the kinetics of the *E*/*Z*-isomerization of azo-guest molecules was investigated.[12,13] Upon irradiation with UV light the equilibrium between the two states is shifted towards the *Z*-state while in a thermal reisomerization process the molecular shape changes from the bend *Z*-isomer back to the rod-like *E*-isomer, which is favoured by the rod-like environment in the LC-matrix. Thus, the activation energy for the thermal *Z*/*E*-reisomerization in the LC host is clearly lower than that in an isotropic host phase as reported by Zentel[12] and Finkelmann.[13] As common azobenzene dyes are often polar or

[a] *Institut für Organische Chemie, Universität Stuttgart, Pfaffenwaldring 55, D-70569 Stuttgart, Germany. E-mail: sabine.laschat@oc.uni-stuttgart.de; Fax: +49 711 685 64285; Tel: +49 711 685 64565*

[b] *Institut für Physikalische Chemie, Universität Stuttgart, Pfaffenwaldring 55, D-70569 Stuttgart, Germany*

† Electronic supplementary information (ESI) available: Anion exchange in chloride **6d·Cl** and DSC measurement of the resulting azobenzene guanidinium salts **6d·X**, photoisomerization of ILC **6c·Cl** in the anisotropic C_{12}MIM-Br matrix, X-ray crystal structure of **6a·Cl** as well as data of all guanidinium salts **6**. CCDC 1030119 and 1030120. For ESI and crystallographic data in CIF or other electronic format see DOI: 10.1039/c4cp04783d

‡ Both coauthors contributed equally to this work.

even ionic their miscibility with non-ionic LCs is rather limited, leading to a demixing of the LC and the azobenzene especially after the photoisomerization to the *Z*-isomer.[14] Ionic liquid crystals (ILCs) are so-called designer solvents, whose properties can easily be tuned by a systematic selection of cations and anions. Thus, to overcome the solubility problem we developed a new approach where an ionic liquid crystal (ILC) matrix is used to investigate the kinetics of the *Z*/*E*-reisomerization of ionic azobenzene molecules. This method may be of particular interest as it would lead to tunable reaction media. For this purpose we synthesized novel guanidinium ILCs which are tethered *via* flexible spacer to the mesogenic azobenzene unit and studied their thermotropic mesomorphic behaviour as well as *E*/*Z*-photoisomerization in an anisotropic and in an isotropic host medium. The results are reported below.

2 Results and discussion

2.1 Synthesis of guanidinium azobenzene ILCs

The synthesis of guanidinium azobenzene ILCs **6** commenced with *p*-nitrophenol (**1**), which was submitted to Williamson etherification with octylbromide followed by Pd-catalyzed hydrogenation to provide 4-octyloxyaniline (**2**) in 91% (Scheme 1).

Subsequent diazotation and azo coupling with phenol following a sequence by Shi[15] yielded 4-hydroxy-4′-(octyloxy)azobenzene (**3**). Its treatment with the known *N*-phthalimido-protected spacer units **4a–f**[16] under Williamson conditions afforded the *N*-phthalimido derivatives **5a–f.** Hydrazinolysis and subsequent reaction with commercially available chloroformamidinium chloride following our previously established method[17] yielded the corresponding guanidinium chlorides **6(a–f)·Cl.** Chloride **6d** with hexyl spacer was also converted *via* salt metathesis[18] to guanidinium ILCs **6d·X** with different anions (X = Br, I, OTf, SCN, BF_4, PF_6) (see ESI†).

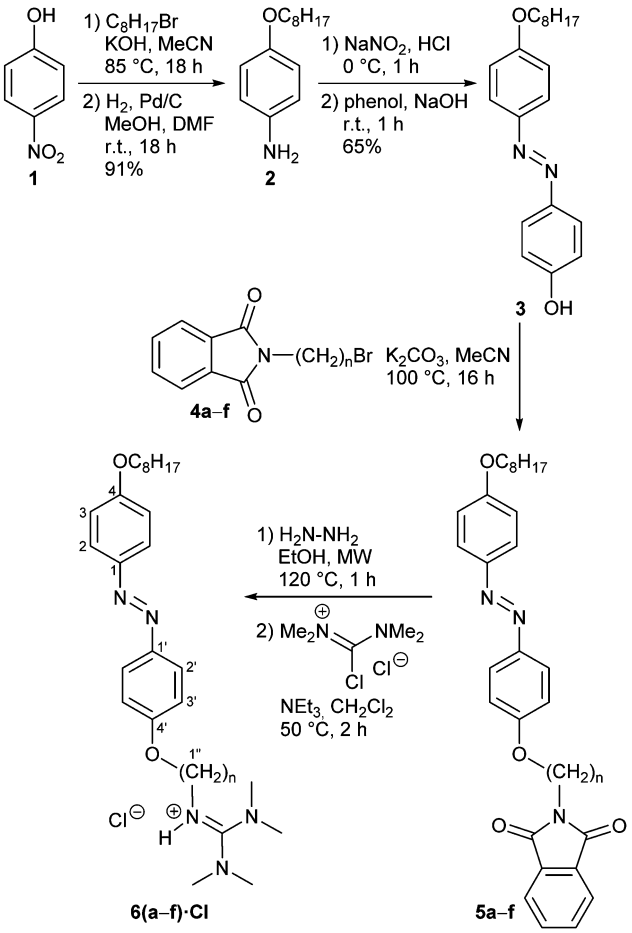

4–6	n	5	yield [%]	6·Cl	yield [%]
a	3	**5a**	76	**6a·Cl**	34
b	4	**5b**	84	**6b·Cl**	65
c	5	**5c**	67	**6c·Cl**	21
d	6	**5d**	88	**6d·Cl**	68
e	7	**5e**	71	**6e·Cl**	72
f	8	**5f**	91	**6f·Cl**	59

Scheme 1 Synthesis of azobenzene guanidinium chlorides **6·Cl**. Numbering for assignment of individual NMR signals.

2.2 Mesomorphic properties of guanidinium azobenzene ILCs

The mesomorphic properties of guanidinium azobenzenes **6·Cl** were determined by differential scanning calorimetry (DSC), polarizing optical microscopy (POM) and X-ray diffraction (wide angle (WAXS) and small angle X-ray scattering (SAXS)).

Under the POM on plain glass plates all compounds **6·Cl** displayed homeotropic textures indicating the presence of SmA phases, as shown in Fig. 1a for guanidinium chloride **6f·Cl** as example.

By filling the samples into polyimide coated LC-cells planar fan-shaped textures could be observed in the SmA phase. In order to suppress photo-induced isomerization, phase transitions were studied under POM using monochromatic light at 656 nm, which made the textures appear red (Fig. 1b). A typical DSC curve with a hysteresis between heating and cooling cycle indicating some degree of supercooling is exemplarily given for chloride **6f·Cl** with octyl spacer (Fig. 2).

The results of the DSC experiments upon third heating and cooling are summarized in Table 1 and illustrated in Fig. 3. All guanidinium azobenzene chlorides **6·Cl** displayed enantiotropic mesomorphism irrespective of the spacer lengths. Within the homologues **6(a–f)·Cl** melting and clearing points increased from **6a·Cl** to a maximum for **6b·Cl** and **6c·Cl** and then decreased continuously for spacer lengths of n = 6–8 (Fig. 3). The mesophase widths, however, remained similar. A comparison of the transition temperatures during heating and cooling also revealed supercooling, thus the phase widths are usually broader in the cooling cycle.

In order to obtain more information about the smectic A mesophase geometry, the guanidinium chlorides **6·Cl** were further characterized by X-ray measurements. The temperature-dependent layer spacings d of the SmA phases of **6(a–f)·Cl** were obtained by small angle X-ray scattering (SAXS) upon cooling (Fig. 4a). All azobenzene ILCs **6·Cl** showed a linear increase of the layer spacings with decreasing temperature being typical for SmA phases. By comparing the phase transition temperatures received from X-ray measurements with the POM observations a broader phase range of the SmA phase due to supercooling

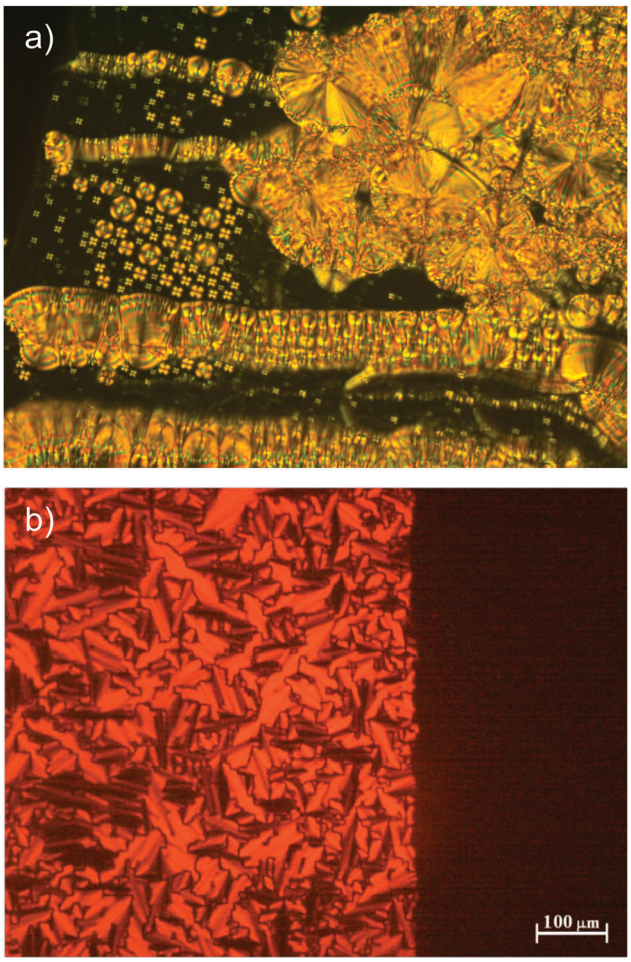

Fig. 1 (a) Homeotropic texture of **6f·Cl** typical for SmA phases at 129 °C as seen between crossed polarizers upon cooling from the isotropic liquid (magnification ×200) and (b) in a LC-cell with polyimide coated glassplates at 133.3 °C and a wavelength filter at 656 nm; left: fan-shaped texture of the planar oriented SmA phase, right: homeotropic orientation.

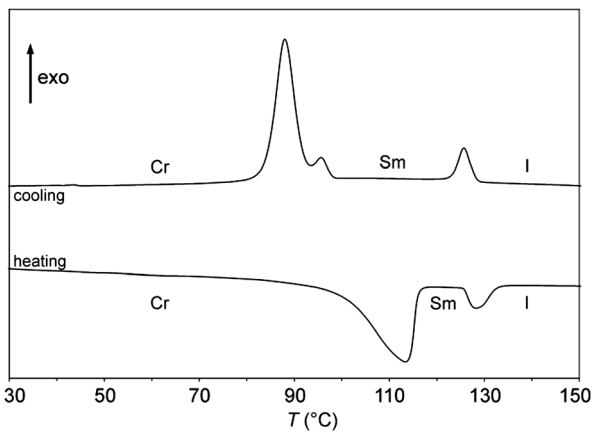

Fig. 2 DSC curves of guanidinium azobenzene ILC **6f·Cl** upon 3 heating and cooling (heating/cooling rate 10 K min^{-1}). Cr = crystalline, Sm = smectic, I = isotropic liquid.

effects could be found especially for **6a·Cl** and **6c·Cl**. In Fig. 4b the smectic layer spacing at the isotropic to SmA phase

Table 1 Phase transition temperatures [°C] (and enthalpies [kJ mol^{-1}]) of guanidinium azobenzene ILCs **6·Cl** upon third heating and cooling cycle[a,b]

Compd	Spacer length n	Cr		SmA		I	Cycle
6a·Cl	3	•	118 (18.9)	•	139 (1.2)	•	Heating
	3	•	—[c]	•	153[c]	•	Cooling
6b·Cl	4	•	125 (27.9)	•	151 (1.0)	•	Heating
	4	•	109 (24.9)	•	153 (1.0)	•	Cooling
6c·Cl	5	•	125 (30.7)	•	150 (1.5)	•	Heating
	5	•	105 (29.3)	•	151 (1.6)	•	Cooling
6d·Cl	6	•	117 (33.1)	•	137 (1.9)	•	Heating
	6	•	95 (6.2)	•	137 (2.0)	•	Cooling
6e·Cl	7	•	111 (19.2)	•	129 (0.4)	•	Heating
	7	•	97 (7.7)	•	134 (0.2)	•	Cooling
6f·Cl	8	•	100 (28.1)	•	125 (3.5)	•	Heating
	8	•	100 (2.5)	•	132 (3.5)	•	Cooling

[a] Phase transitions were determined by DSC (heating/cooling rate 10 K min^{-1}). [b] The following phases were observed: crystalline (Cr), smectic A (SmA), isotropic (I). [c] The phase transitions could not be determined by DSC; the given temperature was obtained by POM. Strong supercooling, however, led to unreproducible data for the SmA → Cr transition. By POM the transition values Cr 130.3 °C SmA 153.5 °C I were observed upon heating.

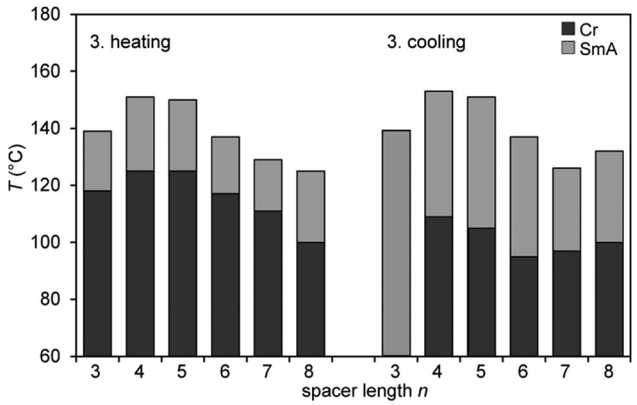

Fig. 3 Mesophase widths of guanidinium azobenzene ILCs **6(a–f)·Cl** depending on the spacer lengths n upon third heating/cooling obtained by DSC (heating/cooling rate 10 K min^{-1}).

transition is plotted against the theoretical values of the molecular lengths that were received from molecular modelling using an energy minimization by a semi empirical force field based on the MM2 basis set (ChemDraw 3D). The relation of the layer spacing d and the calculated molecular length l_{opt} showed a quite linear behaviour (Fig. 4b). The layer spacing was found to be about 1.4 times the molecular length indicating the formation of partial bilayers with interdigitated molecules.

SAXS measurements also allow the calculation of the translational order parameter Σ of the SmA phase providing a measure for the quality of the translational periodicity of the smectic layers. Σ was calculated in the SmA phase by extrapolation of the integrated temperature-dependent scattering intensity of the layer peak to absolute zero by using our previously developed method.[19] The determined smectic order parameters for **6c·Cl**, **6e·Cl**, and **6f·Cl** show quite high values of up to 0.9 (Fig. 5) compared to conventional thermotropic liquid crystals which usually ranged around 0.7.[20] The high value of the translational order in the

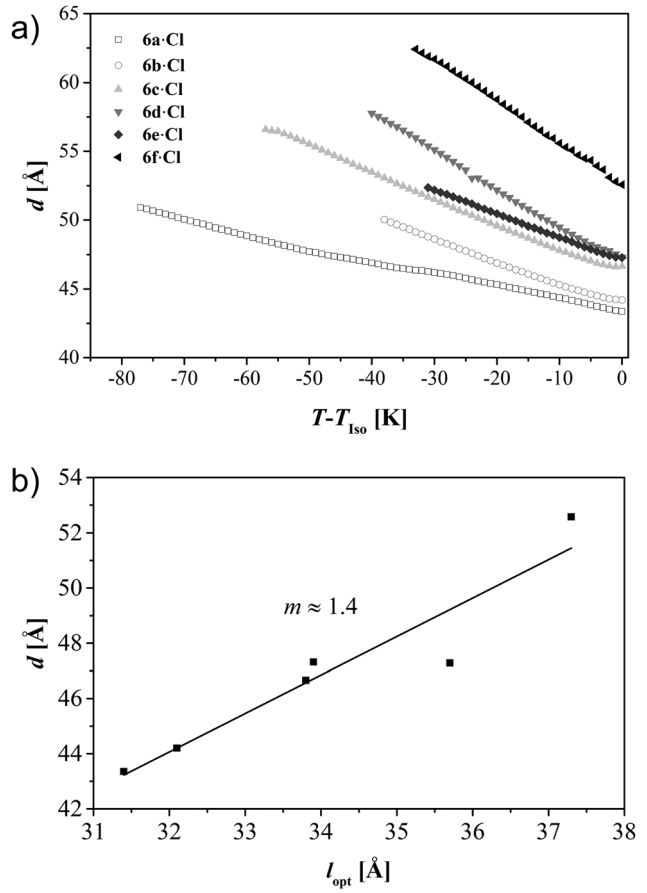

Fig. 4 (a) Smectic layer spacing d in the SmA phase *vs.* the temperature difference to the isotropic phase $T-T_{iso}$. (b) Smectic layer spacing d at the isotropic to SmA phase transition plotted against the modelled molecular length (l_{opt}) of chlorides **6(a–f)·Cl** by using ChemDraw 3D.

mesogens **6·Cl** implies that the molecules are only little dislocated out of the partial double layers. This might be due to a strong segregation tendency of the ionic head group from the non-ionic part of the mesogens which try to avoid each other.

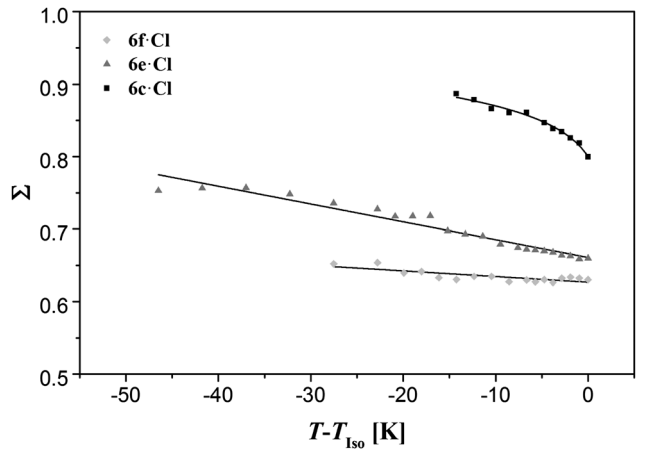

Fig. 5 Translational order parameters Σ in the SmA phase of ILCs **6c·Cl**, **6e·Cl**, and **6f·Cl** in dependence on the temperature difference to the isotropic phase transition $T-T_{iso}$.

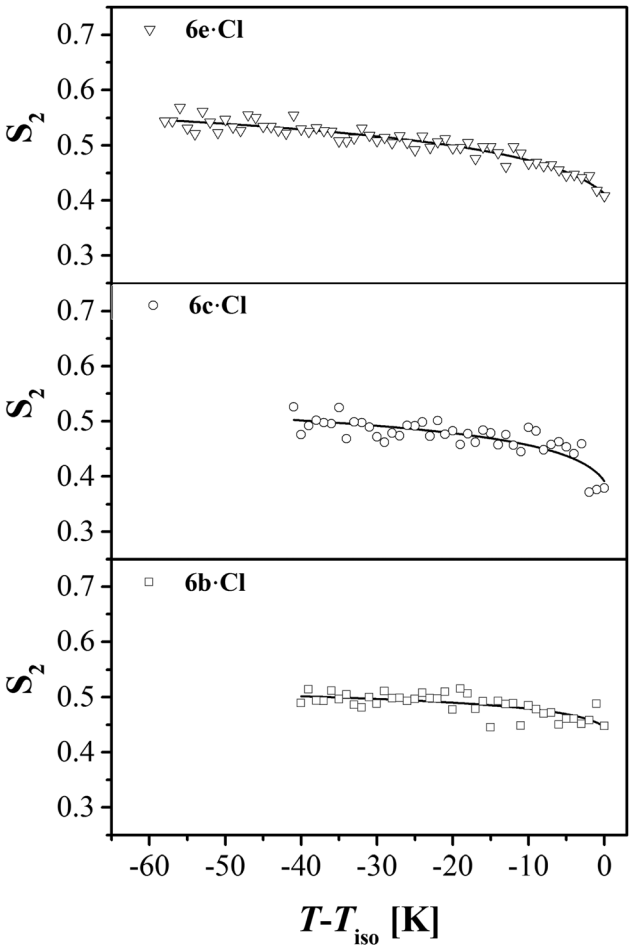

Fig. 6 Orientational order parameters S_2 in the smectic A phase of mesogens **6b·Cl**, **6c·Cl** and **6e·Cl** in dependence on the temperature difference to the isotropic phase transition $T-T_{iso}$.

The influence of the spacer length on the parallel orientation of the molecules was investigated by determining the orientational order parameters S_2 in the mesophase of azobenzene ILCs **6b·Cl, 6c·Cl** and **6e·Cl.** These parameters S_2 were derived from the diffuse wide angle X-ray scattering arcs using the method by Davidson and Levelut.[21]

The measurements were performed at a smectic monodomain in the sample (uniform orientation of the layer normal and director). The samples of mesogens **6b·Cl, 6c·Cl** and **6e·Cl** exhibit orientational order parameters S_2 in the range of 0.5 (Fig. 6), thus no dependence on the spacer length could be observed.

S_2 values of 0.5 are quite low for a smectic mesophase. Usually values around 0.7 are found in thermotropic liquid crystals.[22] The low orientational together with the high translational order in the mesophases of ILCs **6·Cl** indicate that the layer formation due to nanosegregation is much more important than the parallel orientation of the molecules. For conventional thermotropic materials the opposite was found.[23]

2.3 Solid state properties of guanidinium azobenzene ILCs

We were able to obtain single crystals of **6b·Br**, which were suitable for X-ray crystal structure analysis (Fig. 7). In the solid

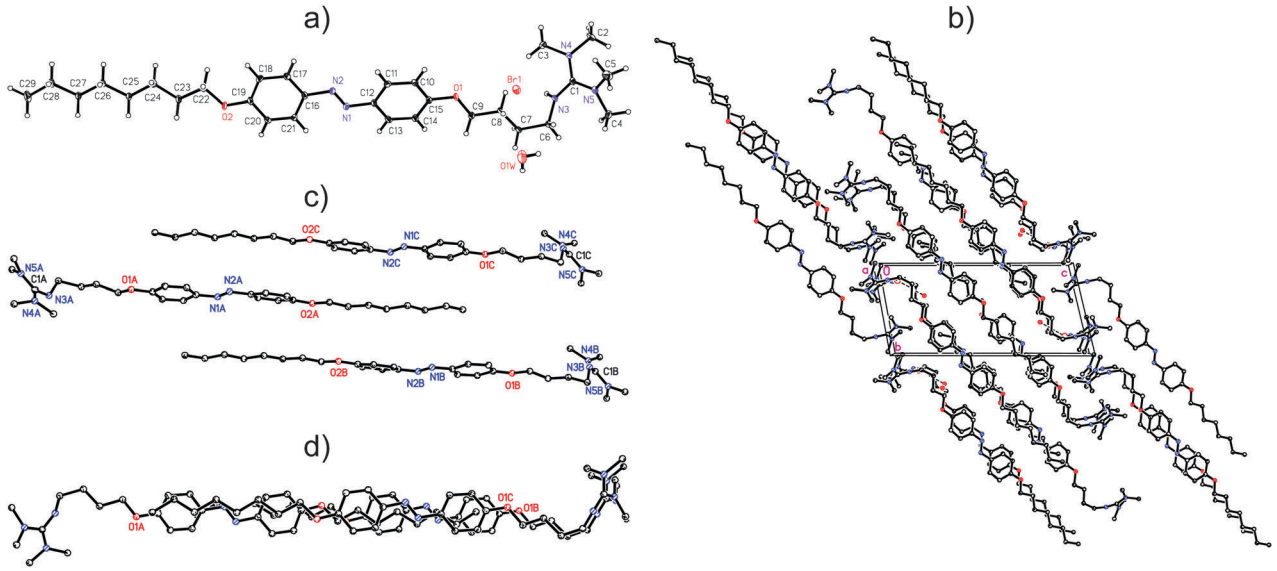

Fig. 7 (a) X-ray structure of **6b·Br** in the solid state (atomic numbering system used only for X-ray diffraction studies). The H1W1–Br1 distance is 2.55(3) Å with an angle O1W–H1W1–Br1 of 175(3)°. The H2W1–N2 distance is 2.28(4) Å with an angle O1W–H2W1–N2 of 165(3)°. The relevant distance H3–Br1 is 2.47 Å and the angle N3–H3–Br1 is 165°. (b) Packing diagram for **6b·Br**. The interdigitation situation of **6b·Br** (only cation) is given in (c) side-view and (d) top-view (hydrogens omitted for clarity).

state **6b·Br** crystallized in the space group $P\bar{1}$ with one ion pair and one water solvent molecule in the asymmetric unit (Fig. 7a). The water builds up intermolecular hydrogen interactions to the bromide ion and to N2 of the azo function. Additionally, the N3–H3 function of the guanidinium head group acts as hydrogen bond donor to the bromide anion as acceptor. In the bc-view of the packing diagram (Fig. 7b) a layer-type stacking of the guanidinium cations is evident with an alternate antiparallel interdigitated orientation (Fig. 7b–d).

The total length of the guanidinium cation is 30.93 Å. In consideration of the interdigitated layer the length is increased to 42.95 Å. The resulting factor of 1.39 (Fig. 7c and d) agreed well with the packing in the liquid crystalline phase. A nearly coplanar orientation of the terminal octyloxy group, both phenyl moieties and the butyl spacer (C6–C9) supports the capability of the cation to interdigitate. The average distance of the nearest atoms between the interdigitated layers is 3.79 Å. In contrast, the C1, N3, N4, N5 guanidinium core shows an interplanar angle of 49.5(1)° to the directly attached butyloxy chain. The packing is stabilized by a number of weak intermolecular electrostatic interactions. Another layer-type orientation is evident with a stacking vector along the *c*-axis building up alternate by the guanidinium head groups and the alkoxyazobenzene chains (Fig. 7b). It should be noted that the X-ray crystal structure analysis of **6b·Cl** which crystallized with one ion pair and two chloroform solvent molecules in the unit cell gave comparable packing results (see ESI†).

2.4 Isomerization of guanidinium azobenzene ILCs in different matrices

A positive influence of a calamitic liquid crystalline (LC) host phase on the reisomerization of a liquid crystalline polymer containing an azobenzene derivative as covalently linked side group from the bend *Z*-isomer to the rod-like *E*-isomer was already reported.[12] Therefore, we were interested to investigate the influence of an ionic liquid crystalline (ILC) host phase on the *E*/*Z*-photoisomerization of the series of homologues **6(a–f)·Cl**. For this purpose the anisotropic ionic smectic A phase of 1-dodecyl-3-methylimidazolium bromide (C_{12}MIM-Br) was used as host and water as isotropic host phase for comparison. Diluted solutions of the azobenzene chlorides **6(a–f)·Cl** in the two host phases were prepared without any miscibility problems. The reisomerization of all samples was studied by using time-resolved UV-Vis spectroscopy in the temperature range of 50–75 °C in either UV-Vis quartz glass cuvettes (d = 1 cm) for aqueous solutions or in commercial polyimide coated liquid crystal cells (thickness 1.6 μm) for ILC–C_{12}MIM-Br mixtures. The mixtures of ILCs **6·Cl** and the host phases were first irradiated with strong UV-light for 20 seconds with a commercially available 75 W UV-lamp to achieve a sufficient shift of the *E*/*Z*-equilibrium towards the *Z*-isomer. UV-Vis spectra were then recorded in specific time intervals to observe the reisomerization to the thermodynamically more stable *E*-isomer. Fig. 8a shows exemplarily the absorption spectra of **6c·Cl** at T = 73.6 °C in water. The increase of the π–π* absorption band of the *E*-isomer with time at 360 nm is clearly visible. The time-dependent behaviour of the absorption at this wavelength was recorded for mesogens **6(a–f)·Cl** at different temperatures in both host phases and was found to follow a first-order kinetics in all samples. The rate constants were therefore obtained from monoexponential fits of the respective curves at different temperatures, as shown for azobenzene **6c·Cl** in water (Fig. 8b). The activation energies (E_A) of derivatives **6(a–f)·Cl** in the two different host phases were calculated from the temperature-dependent rate constants by using an Arrhenius plot. The activation energies for **6(a–f)·Cl** obtained in the anisotropic ILC and in water as isotropic solution were compared in Fig. 8c (for measurements of **6·Cl** in the ILC host see the ESI†).

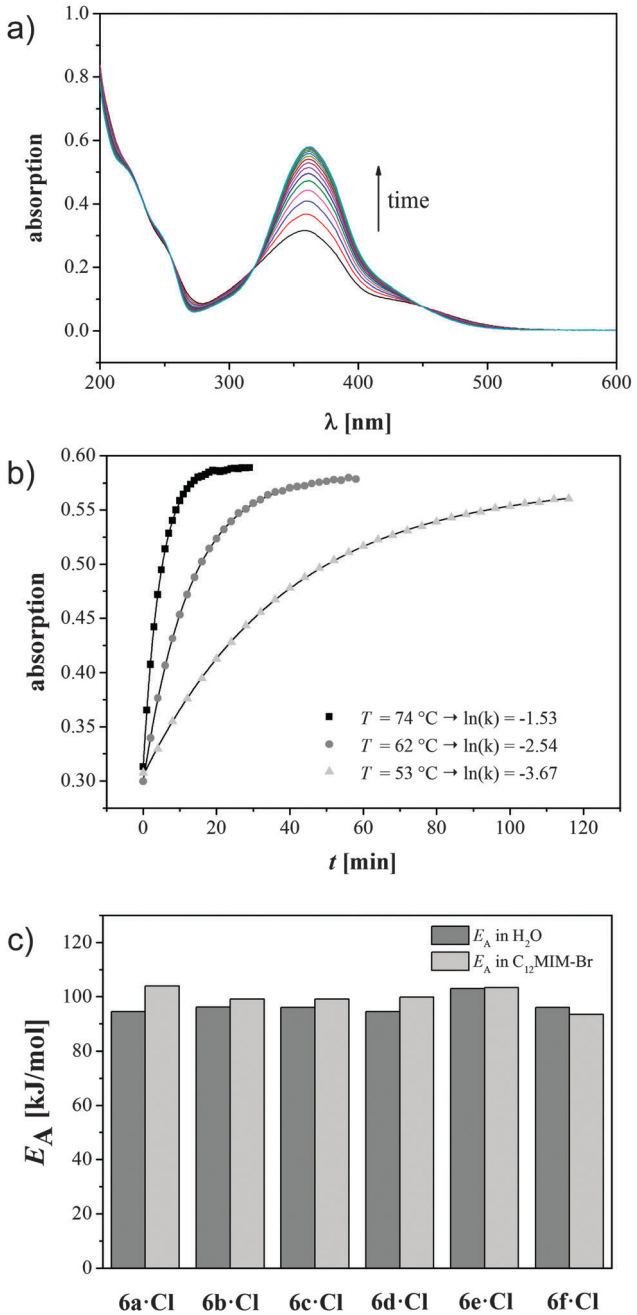

Fig. 8 Photoisomerization experiments of ILCs **6·Cl**. (a) Wavelength-dependent absorption spectra of **6c·Cl** in aqueous solution during the *E*/*Z*-reisomerization at T = 73.6 °C. (b) UV-Vis absorption at 360 nm *vs.* time curves for **6c·Cl** in water (symbols) as well as the mono exponential fit curves (black solid lines) for different temperatures and the obtained rate constants. (c) Activation energies E_A for the *Z*/*E*-reisomerization of mesogens **6(a–f)·Cl** in the two different host phases.

The activation energies were similar irrespective of the spacer lengths n and of the host phase, thus, both the alkyl chain and the host seem to have only little influence on the *E*/*Z*-isomerization. For the aqueous solution a slightly lower activation energy by average can be found than for the anisotropic SmA phase of C_{12}MIM-Br. This could be due to the fact that the small polar water molecules may stabilize the transition state of the *E*/*Z*-isomerization better

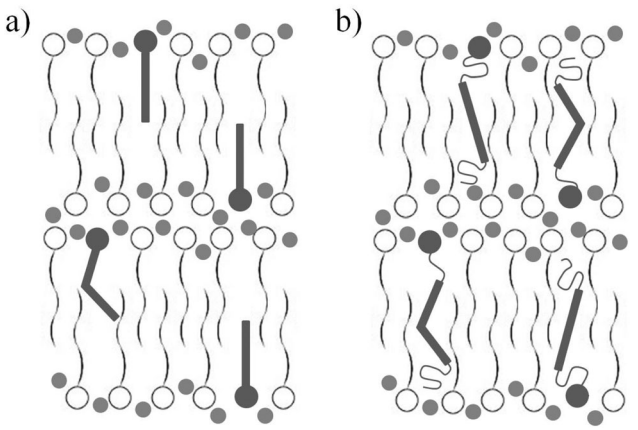

Fig. 9 Schematic drawing of an ionic liquid crystalline host phase doped with azo guest molecules. (a) The length of the guest molecules is shorter than the layer spacing of the matrix. Therefore, the *E*-isomer of the azo compounds can be easily accommodated in the host without any steric hindrance. (b) The guest molecules are longer than the layer spacing of the matrix, consequently they need to be kinked to fit into the smectic layers of the host.

than the bulkier ionic molecules of C_{12}MIM-Br which are furthermore locked in the nanosegregated layers. In addition the differences in size between guest and host molecules might inhibit the reduction of E_A in the ordered SmA phase compared to the isotropic medium water. The C_{12}MIM-Br molecules show a layer spacing of their bilayers of 27.5–29 Å, the azobenzene guest molecules **6·Cl**, however, possess molecular lengths of already 31–37 Å for a single molecule and layer spacings in their bilayers are in between 45 and 65 Å. Therefore, the guest molecules might just simply be too long to fit into the layers of the host matrix and thus, stabilization of the rod-like *E*-isomer in the SmA matrix cannot occur. The two cases that might occur by adding an ionic guest molecule into an ionic matrix are depicted in Fig. 9.

When the guest molecules are shorter than the layer spacing of the matrix they fit well into the layers and the *E*-isomer is stabilized by the rod-like anisotropic environment of the matrix (Fig. 9a). In this case, the activation energy of the *Z*/*E*-reisomerization should be reduced compared to an isotropic matrix. In Fig. 9b the guest molecules are longer than the layer spacing of the matrix. Due to nanosegregation an ionic sheet is formed between two double layers. This ionic layer might act as a barrier preventing the guest molecules from compensating their long length by out-of-layer fluctuations like it is known from non-ionic bidisperse thermotropic liquid crystals.[24] Therefore the guest molecules are kinked to fit into the layers. This kinked form of the azo-mesogens is assumed to be responsible for the loss of positive influence of the rod-like matrix on the stabilisation of the rod-like *E*-isomer. This might explain why no decrease of the activation energies of the *E*/*Z*-reisomerization of azobenzene ILCs **6·Cl** could be found in the (C_{12}MIM-Br) matrix compared to the isotropic medium water.

A second possibility may arise from the very low orientational order in the hydrophilic alkyl sublayer of the smectic A phase of the host C_{12}MIM-Br. The two sharp Bragg peaks (Fig. 10) in the small angle regime indicate a nearly perfect alignment of the

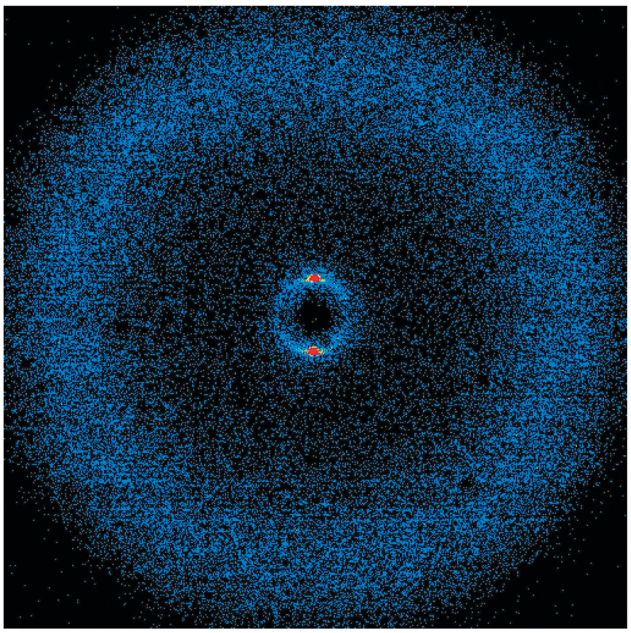

Fig. 10 2D WAXS diffractogram of an aligned sample of C_{12}MIM-Br in the SmA phase at 100 °C. While the smectic layer peaks in the small angle regime exhibits two sharp maxima in dependence on the azimuthal angle, no angular-dependence could be found for the broad reflex in the wide angle regime. Explanations see text.

smectic layers with an almost uniform direction of the layer normal. The orientational order of the alkyl chains is reflected by the azimuthal distribution of the diffuse wide angle scattering, that, however, does not show any significant azimuthal modulation, similar to the scattering of an isotropic fluid. The 2D X-ray pattern confirms the absence of significant orientational order of the alkyl tails in the hydrophobic SmA sublayer of C_{12}MIM-Br and *E*/*Z*-reisomerization therefore takes place in a mainly isotropic environment leading to only marginal differences in the activation energy in comparison to water. A similar finding of highly disordered alkyl chains in the smectic phase of a viologen-based ILC was recently reported by Saielli.[25]

3 Conclusions

A series of novel guanidinium azobenzene ILCs **6·Cl** was prepared and both the solid state behaviour and the liquid crystalline properties studied. WAXS and SAXS data revealed a SmA phase with interdigitated bilayers, that was in good agreement with single-crystal X-ray structure analysis of two derivatives.

The reaction kinetics of the azo *Z*/*E*-reisomerization of ILCs **6·Cl** in the different hosts H_2O and C_{12}MIM-Br was investigated. A good miscibility of the ionic azobenzene molecules in both host phases was observed. In aqueous isotropic solution the ionic mesogens **6(a–f)·Cl** showed similar activation energies in the range of 97 kJ mol^{-1} independent of their spacer lengths. The same result was found for mixtures with the anisotropic host medium C_{12}MIM-Br, in which the average E_A was 100 kJ mol^{-1}. Thus, no activation energy decrease was realized by using the anisotropic host. This result is in contrast to previous findings by Finkelmann[13] which revealed that a flexible anisotropic environment of a nematic phase reduced the activation energy of the *Z*/*E*-reisomerization. On the other hand Zentel[12] was able to demonstrate this effect also for the relatively rigid anisotropic environment of a LC polymer with azo compound as part of the polymer network. Presumably, in our case a steric misfit of the ILC host and the azo ILC guest as well as the very low orientational order of the hydrophobic alkyl sublayer of the ILC host might counteract rapid *Z*/*E*-reisomerization. In order to clarify this, future work utilizing combinations of azo ILC guests and ILC hosts of similar size must be carried out. Furthermore, ILCs with a mesogenic core exhibiting higher orientational order parameters than ILCs without mesogenic cores, should be used as hosts to investigate the influence of the orientational order on the *E*/*Z*-reisomerization. On the other hand, *Z*/*E*-isomerization kinetics of azo ILC guests in ILC hosts with an even larger mismatch of the molecular length as compared to ours might further increase the activation barrier and thus result in the kinetic stabilization of the *Z*-isomer. This would be relevant for future applications of ILCs as reaction media.

4 Experimental section

4.1 Materials and instrumentation

^{1}H and ^{13}C NMR spectra were recorded on a Bruker Avance DPX 250, Avance 300 and Avance 500 (tetramethylsilane as internal standard). ^{13}C multiplicities were assigned by DEPT experiments. Variable temperature NMR spectra were acquired on a Bruker Avance 50. IR spectra were recorded on a Bruker Vector 22 FT-IR spectrometer with ATR technique. Mass spectrometry was performed on a Varian MAT 711 mass spectrometer with EI ionization (70 eV), a Finnigan MAT 95 with CI ionization using methane as reactant gas and a Bruker micrOTOF_Q with electrospray ionization. Elemental analyses were performed on a Carlo Erba Strumentazione Elemental Analyzer Model 1106. Column chromatography was performed using silica gel 60 (Fluka, mesh 40–63 μm). Single-crystal X-ray structure analyses were performed on a Bruker kappa APEX II Duo diffractometer (λ = 0.71073 Å) at 100 K. Differential scanning calorimetry was performed using a Mettler Toledo DSC822. Optical polarizing microscopy was performed using an Olympus BX 50 polarizing microscope combined with a Linkam LTS 350 hot stage and a Olympus BH2 polarizing microscope equipped with a Linkam LTS 350 hot stage and a Scope Tek DCM 500 digital camera.

All air sensitive reactions were carried out under nitrogen using standard Schlenk techniques. All chemicals used were commercially available and used without further purification, unless otherwise noted. Reactions under microwave irradiation were carried out in a CEM Explorer in closed vials under isothermal conditions. 1-Dodecyl-3-methylimidazolium bromide was prepared according to known procedures[26] and showed the expected physical and spectral properties.

X-ray diffraction. Wide angle X-ray measurements on aligned samples (magnetic field ~ 1 T) at variable temperatures were

performed with a Bruker AXS Nanostar C (Ni filtered CuK_α, λ = 1.5418 Å, with crossed Göbel-mirrors as monochromator). The diffraction patterns were recorded on a real-time 2D-detector (HI-STAR, Bruker). The samples were filled into Mark capillary tubes (0.7 mm outside diameter) from Fa. Hildenberg GmbH and tempered in a temperature-controlled sample holder (Eurotherm, with a control from mri, Physikalische Geräte GmbH). A Kratky compact camera and a SAXSess-System from Anton Paar were used to perform small-angle X-ray scattering (Ni-filtered CuK_α radiation with wavelength λ = 1.5418 Å) The unaligned samples were filled into Mark capillary tubes of 0.7 mm diameter and put into a temperature controlled sample holder (Anton Paar). The SAXSess is equipped with a CCD detector, the Kratky compact camera uses a one-dimensional electronic detector by M. Braun.

UV-Vis spectroscopy. Solutions of azobenzene ILCs **6·Cl** in H_2O (*ca.* 0.0018 wt% ILC) and in C_{12}MIM-Br (1.5–3.5 wt% ILC) were prepared. UV-Vis spectra in aqueous solution were recorded on a Perkin-Elmer Lambda25 spectrometer equipped with a PTP-1 Peltier system (Perkin-Elmer) for heating and cooling. The samples were filled into quartz glass cuvettes with 1 cm thickness (Hellma).The UV-Vis spectra in the ILC host were recorded on a Perkin-Elmer Lambda2 spectrometer equipped with a homemade temperature control. The samples were filled into commercially available liquid crystal cells from AWAT PPW, Poland. The thickness of the cells was 1.6 μm. The samples were irradiated with a 75 W UV-lamp (Q LUX pro V from Rolence Enterprise Co. Ltd).

4-Octyloxyaniline (2). To a solution of **1** (34.0 g, 134 mmol) in acetonitrile (0.7 L) were added KOH (8.20 g, 147 mmol) and then 1-bromooctane (27.4 g, 141 mmol) and the reaction mixture was heated at 85 °C for 45 h. The solvent was evaporated *in vacuo* and the residue was suspended in H_2O (100 mL) and extracted with CH_2Cl_2 (3 × 100 mL). The combined extracts were dried ($MgSO_4$) and the solvent was evaporated *in vacuo*. The residue was purified by destillation (b.p. 130 °C/0.02 mbar), followed by recrystallization from MeOH to give 4-octyloxynitrobenzene as a pale yellow solid (32.8 g, 93%).

To a solution of 4-octyloxynitrobenzene (10.2 g, 41 mmol) in MeOH/DMF (1 : 1) was added under inert atmosphere Pd on carbon (0.28 g, 260 mmol, 10% Pd) and hydrogen was bubbled through the mixture under vigorous stirring at r.t. for 18 h. The mixture was filtered over celite and the solvent was removed to give **2** as a brown crystalline solid (8.42 g, 38 mmol, 91%). Spectroscopic data are in accordance with those in the literature.[27]

4-Hydroxy-4′-(octyloxy)azobenzene (3). A solution of **2** (25.2 g, 114 mmol) in 2 M HCl (140 mL) was cooled to −3 °C. Then 2 M $NaNO_2$ (60 mL, 116 mmol) was added dropwise at 0 °C. After stirring for 30 min, urea (87 mg, 1.4 mmol) was added and the resulting mixture was dropwise added to a cooled solution of phenol (11.3 g, 114 mmol) in 2 M NaOH (114 mL, 228 mmol) and stirring was continued for 1 h. The resulting brown precipitate was collected on a fritted funnel, suspended in hot acetic acid and filtered. Upon storage of the filtrate overnight at 0 °C a brown solid precipitated from the solution, which was isolated and washed with *n*-hexane to yield **3** as a brown powder (24.2 g, 74 mmol, 58%). Mp 103 °C (103–103.5 °C[28]). Spectroscopic data are in accordance with those in the literature.[27]

General procedure for the preparation of 2-[ω-{(4-(*E*)-[4-(octyloxy)phenyl]diazenyl}phenoxy)alkyl]-1*H*-isoindole-1,3(2*H*)-diones 5. To a suspension of **3** (0.60 g, 1.80 mmol) and K_2CO_3 (1.40 g, 10.0 mmol) in acetonitrile (20 mL) was added the respective *N*-(ω-bromoalkyl)phthalimide **4** (2.00 mmol) and the resulting mixture was refluxed for 18 h. After removal of the solvent *in vacuo*, the crude product was dissolved in CH_2Cl_2 (50 mL), filtered, concentrated *in vacuo* and recrystallized from acetonitrile.

2-[3-{(4-(*E*)-[4-(Octyloxy)phenyl]diazenyl}phenoxy)propyl]-1*H*-isoindole-1,3(2*H*)-dione (5a). Yellow crystalline solid (120 mg, 0.34 mmol, 76%), mp 129 °C. FT-IR (ATR) $\tilde{\nu}$/cm^{-1} 2921s, 2852m, 1768m, 1712vs, 1592s, 1499m, 1465m, 1391s, 1372m, 1328w, 1254vs, 1186w, 1145vs, 1109w, 1169m, 970w, 942m, 903w, 870w, 841vs, 815w, 787w, 720vs, 641w, 622w, 577w, 550s, 535m, 507m. ^{1}H-NMR (500 MHz, $CDCl_3$): δ = 0.89 (t, J = 6.9 Hz, 3H, CH_3), 1.24–1.39 (m, 8H, CH_2), 1.44–1.51 (m, 2H, CH_2), 1.79–1.84 (m, 2H, CH_2), 2.20–2.25 (m, 2H, $OCH_2CH_2CH_2N$), 3.93 (t, J = 6.8 Hz, 2H, 1″-H), 4.02 (t, J = 6.4, 2H, OCH_2), 4.11 (t, J = 6.0, 2H, NCH_2), 6.88 (d, J = 6.9 Hz, 2H, 3-H), 6.98 (d, J = 6.9 Hz, 2H, 3′-H), 7.71–7.73 (m, 2H, 2-H), 7.80–7.83 (m, 2H, 2′-H), 7.84–7.86 (m, 4H, 3″-H, 4″-H) ppm. ^{13}C-NMR (125 MHz, $CDCl_3$): δ = 14.1 (CH_3), 22.7, 26.0, 28.3, 29.2, 29.2, 29.4, 31.8 (CH_2), 35.5 (N-CH_2), 66.0 (C-1″), 68.3 (C-CH_2O), 114.6 (C-3′), 114.6 (C-3), 123.3 (C-3″), 124.3 (C-2′), 124.3 (C-2), 132.2 (C-2″), 134.0 (C-4″), 146.9 (C-1′), 147.1 (C-1), 160.6 (C-4′), 161.2 (C-4), 168.4 (C═O) ppm. MS (ESI): m/z 393.30, 514.27 $[M]^+$, 536.25 $[M + Na]^+$. HRMS (ESI): calcd for $[C_{31}H_{35}N_3O_4 + Na]^+$ 536.2520, found 536.2505 $[M + Na]^+$. Found: C, 72.49; H, 6.84; N, 8.18. Calcd for $C_{31}H_{35}N_3O_4$: C, 72.49; H, 6.87; N, 8.18%.

2-[4-{(4-(*E*)-[4-(Octyloxy)phenyl]diazenyl}phenoxy)butyl]-1*H*-isoindole-1,3(2*H*)-dione (5b). Yellow crystalline solid (0.14 g, 0.27 mmol, 84%), mp 154 °C. FT-IR (ATR) $\tilde{\nu}$/cm^{-1} 2925s, 2854m, 1771w, 1697vs, 1700s, 1578s, 1494m, 1474m, 1465w, 1435w, 1397s, 1360m, 1316m, 1297w, 1241vs, 1188w, 1144vs, 1106m, 1070w, 1041s, 999m, 966w, 948w, 892w, 868w, 844vs, 777w, 760w, 714vs, 640w, 608w, 553s, 530s. ^{1}H-NMR (250 MHz, $CDCl_3$): δ = 0.89 (t, J = 6.9 Hz, 3H, CH_3), 1.29–1.47 (m, 10H, CH_2), 1.76–1.91 (m, 6H, CH_2), 3.79 (t, J = 6.5 Hz, 2H, 1″-H), 4.02–4.09 (m, 4H, OCH_2, NCH_2), 6.95–7.00 (m, 4H, 3-H, 3′-H), 7.69–7.74 (m, 2H, 2-H), 7.82–7.87 (m, 6H, 2′-H, 3″-H, 4″-H) ppm. ^{13}C-NMR (125 MHz, $CDCl_3$): δ=14.1 (CH_3), 22.7, 25.3, 26.0, 26.6, 28.3, 29.2, 29.4, 31.8 (CH_2), 37.6 (N-CH_2), 67.4 (C-1″), 68.3 (C-CH_2O), 114.7 (C-3′, 3), 123.2 (C-3″), 124.3 (C-2′, C-2), 132.1 (C-2″), 134.0 (C-4″), 146.9 (C-1′), 147.1 (C-1), 160.6 (C-4′), 161.2 (C-4), 168.4 (C═O) ppm. MS (ESI): m/z 528.29, 514.27 $[M]^+$, 550.27 $[M + Na]^+$. HRMS (ESI): calcd for $[C_{32}H_{37}N_3O_4 + Na]^+$ 550.2676, found 550.2688 $[M + Na]^+$. Found: C, 72.86; H, 7.03; N, 7.90. Calcd for $C_{32}H_{37}N_3O_4$: C, 72.84; H, 7.07; N, 7.96%.

2-[5-{(4-(*E*)-[4-(Octyloxy)phenyl]diazenyl}phenoxy)pentyl]-1*H*-isoindole-1,3(2*H*)-dione (5c). Yellow crystalline solid (0.60 g, 1.12 mmol, 67%), mp 119 °C. FT-IR (ATR): $\tilde{\nu}$/cm^{-1} 2922s, 2855m, 1782w, 1770w, 1709vs, 1598s, 1579s, 1496m, 1466m, 1401s, 1332w, 1315w, 1297w, 1242vs, 1146s, 1107m, 1064m, 1046m, 1024m, 1007m, 962m, 901w, 880w, 842vs, 776w, 720s, 705s, 640w, 625w, 552s, 531s. ^{1}H-NMR (250 MHz, $CDCl_3$): δ = 0.89 (t, J = 6.9 Hz, 3H, CH_3), 1.29–1.60 (m, 12H, CH_2), 1.72–1.90 (m, 6H, CH_2), 3.73

(t, J = 7.1 Hz, 2H, 1″-H), 3.99–4.05 (m, 4H, OCH_2, NCH_2), 6.94–7.00 (m, 4H, 3-H, 3′-H), 7.69–7.74 (m, 2H, 2-H), 7.82–7.87 (m, 6H, 2′-H, 3″-H, 4″-H) ppm. ^{13}C-NMR (63 MHz, $CDCl_3$): δ = 14.1 (CH_3), 22.7, 23.4, 26.0, 28.3, 28.8, 29.2, 29.4, 31.8 (CH_2), 37.8 (N-CH_2), 67.9 (C-1″), 68.3 (C-CH$_2$O), 114.6 (C-3′), 114.6 (C-3), 123.2 (C-3″), 124.3 (C-2′, C-2), 132.1 (C-2″), 133.9 (C-4″), 146.9 (C-1′), 147.0 (C-1), 161.0 (C-4′), 161.2 (C-4), 168.5 (C═O) ppm. MS (ESI): m/z 542.30 $[M]^+$, 564.28 $[M + Na]^+$. HRMS (ESI): calcd for $[C_{33}H_{39}N_3O_4 + Na]^+$ 564.2833, found 564.2833 $[M + Na]^+$. Found: C, 73.11; H, 7.30; N, 7.65. Calcd for $C_{33}H_{39}N_3O_4$: C, 73.17; H, 7.26; N, 7.76%.

2-[6-{(4-(*E*)-[4-(Octyloxy)phenyl]diazenyl}phenoxy)hexyl]-1*H*-isoindole-1,3(2*H*)-dione (5d). Yellow crystalline solid (0.14 g, 0.25 mmol, 88%), mp 115 °C. FT-IR (ATR): $\tilde{\nu}$/cm^{-1} 2925s, 2850m, 1770m, 1711vs, 1597s, 1578s, 1498m, 1466m, 1433w, 1394s, 1366m, 1329w, 1311w, 1298w, 1238vs, 1146s, 1106w, 1015w, 986w, 960w, 926w, 896w, 872w, 840vs, 799w, 777w, 719vs, 640w, 620w, 550s, 530s. ^{1}H-NMR (250 MHz, $CDCl_3$): δ = 0.89 (t, J = 6.9 Hz, 3H, CH_3), 1.29–1.57 (m, 14H, CH_2), 1.70–1.87 (m, 6H, CH_2), 3.71 (t, J = 7.2 Hz, 2H, 1″-H), 3.99–4.05 (m, 4H, OCH_2, NCH_2), 6.94–7.00 (m, 4H, 3-H, 3′-H), 7.68–7.73 (m, 2H, 2-H), 7.81–7.88 (m, 6H, 2′-H, 3″-H, 4″-H) ppm. ^{13}C-NMR (63 MHz, $CDCl_3$): δ = 14.1 (CH_3), 22.7, 25.7, 26.0, 26.6, 28.5, 29.0, 29.2, 29.4, 31.8 (CH_2), 37.9 (N-CH_2), 68.1 (C-1″), 68.3 (C-CH$_2$O), 114.6 (C-3′, 3), 123.2 (C-3″), 124.3 (C-2′, C-2), 132.1 (C-2″), 133.9 (C-4″), 146.9 (C-1′, C-1), 161.1 (C-4′), 161.2 (C-4), 168.5 (C═O) ppm. MS (ESI): m/z 556.32 $[M]^+$, 578.30 $[M + Na]^+$. HRMS (ESI): calcd for $[C_{34}H_{41}N_3O_4 + Na]^+$ 578.2989, found 578.2982 $[M + Na]^+$. Found: C, 73.38; H, 7.38; N, 7.50. Calcd for $C_{34}H_{41}N_3O_4$: C, 73.49; H, 7.44; N, 7.56%.

2-[7-{(4-(*E*)-[4-(Octyloxy)phenyl]diazenyl}phenoxy)heptyl]-1*H*-isoindole-1,3(2*H*)-dione (5e). Yellow crystalline solid (0.65 g, 1.14 mmol, 71%), mp 110 °C. FT-IR (ATR): $\tilde{\nu}$/cm^{-1} 2939m, 2921s, 2853m, 1768m, 1707vs, 1598m, 1577s, 1498m, 1466s, 1438w, 1394m, 1372m, 1294w, 1140s, 1106m, 1152m, 1123m, 999w, 933m, 923w, 869w, 842s, 839s, 810w, 778m, 718s, 707m, 639w, 619m, 558m, 548s, 530s. ^{1}H-NMR (250 MHz, $CDCl_3$): δ = 0.89 (t, J = 6.9 Hz, 3H, CH_3), 1.29–1.48 (m, 16H, CH_2), 1.65–1.84 (m, 6H, CH_2), 3.69 (t, J = 7.2 Hz, 2H, 1″-H), 3.99–4.05 (m, 4H, OCH_2, NCH_2), 6.95–7.00 (m, 4H, 3-H, 3′-H), 7.68–7.73 (m, 2H, 2-H), 7.82–7.87 (m, 6H, 2′-H, 3″-H, 4″-H) ppm. ^{13}C-NMR (63 MHz, $CDCl_3$): δ = 14.1 (CH_3), 22.7, 25.9, 26.0, 26.8, 28.5, 28.9, 29.1, 29.2, 29.4, 31.8 (CH_2), 38.0 (N-CH_2), 68.2 (C-1″), 68.3 (C-CH$_2$O), 114.6 (C-3′, 3), 123.2 (C-3″), 124.3 (C-2′, C-2), 132.2 (C-2″), 133.9 (C-4″), 146.9 (C-1′, C-1), 161.1 (C-4′), 161.2 (C-4), 168.5 (C═O) ppm. MS (ESI): m/z 570.33 $[M]^+$, 592.31 $[M + Na]^+$; HRMS (ESI): calcd for $[C_{35}H_{43}N_3O_4 + Na]^+$ 592.3146, found 592.3139 $[M + Na]^+$. Found: C, 73.77; H, 7.66; N, 7.08. Calcd for $C_{35}H_{43}N_3O_4$: C, 73.78; H, 7.61; N, 7.38%.

2-[8-{(4-(*E*)-[4-(Octyloxy)phenyl]diazenyl}phenoxy)octyl]-1*H*-isoindole-1,3(2*H*)-dione (5f). Yellow crystalline solid (0.96 g, 1.60 mmol, 91%), mp 107 °C. FT-IR (ATR): $\tilde{\nu}$/cm^{-1} 2925s, 2854m, 1773m, 1713vs, 1599s, 1579s, 1498m, 1464m, 1434w, 1395s, 1364m, 1334w, 1316w, 1298w, 1240vs, 1187w, 1146s, 1105m, 1088w, 1055m, 1041m, 1021m, 953w, 878w, 841vs, 801w, 778w, 720vs, 641w, 625w, 551s, 531s. ^{1}H-NMR (250 MHz, $CDCl_3$): δ = 0.89 (t, J = 6.9 Hz, 3H, CH_3), 1.29–1.47 (m, 18H, CH_2), 1.62–1.84 (m, 6H, CH_2), 3.68 (t, J = 7.2 Hz, 2H, 1″-H), 3.98–4.05 (m, 4H, OCH_2, NCH_2), 6.96–7.00 (m, 4H, 3-H, 3′-H), 7.68–7.73 (m, 2H, 2-H), 7.80–7.87 (m, 6H, 2′-H, 3″-H, 4″-H) ppm. ^{13}C-NMR (63 MHz, $CDCl_3$): δ = 14.1 (CH_3), 22.7, 25.9, 26.0, 26.8, 28.6, 29.1, 29.2, 29.2, 29.4, 31.8 (CH_2), 38.0 (N-CH_2), 68.2 (C-1″), 68.3 (C-CH$_2$O), 114.6 (C-3′, 3), 123.2 (C-3″), 124.3 (C-2′, C-2), 132.2 (C-2″), 133.8 (C-4″), 146.9 (C-1′, C-1), 161.1 (C-4′), 161.2 (C-4), 168.5 (C═O) ppm. MS (ESI): m/z 427.16, 584.35 $[M]^+$, 606.33 $[M + Na]^+$. HRMS (ESI): calcd for $[C_{36}H_{45}N_3O_4 + Na]^+$ 606.3302, found 606.3320 $[M + Na]^+$. Found: C, 73.90; H, 7.71; N, 7.29. Calcd for $C_{36}H_{45}N_3O_4$: C, 74.07; H, 7.77; N, 7.20.

General procedure for the preparation of *N*-[ω-(4-{(*E*)-[4-(octyloxy)phenyl]diazenyl}phenoxy)alkyl]tetramethylguanidinium chlorides 6(a–f)·Cl. A solution of respective **5** (0.41 mmol) in EtOH (5 mL) was treated with hydrazine hydrate (200 μL, 4.10 mmol, 100%) at 120 °C under microwave irradiation for 1 h. The resulting yellow precipitate was collected *via* a fritted funnel, washed with EtOH and the amine used without further purification.

To a suspension of the amine (1.00 mmol) in CH_2Cl_2 (1 mL) tetramethylchloroformamidinium chloride (12.5 mL, 1.25 mmol, 0.1 M in CH_2Cl_2) was added dropwise, followed by dropwise addition of NEt_3 (0.2 mL, 1.4 mmol) at 50 °C and the resulting mixture was stirred for 2 h. After cooling to r.t., the mixture was concentrated *in vacuo* and the residue was dissolved in CH_2Cl_2 and extracted with 2 M HCl. The organic layer was separated, dried ($MgSO_4$) and concentrated *in vacuo*. The crude product was purified by chromatography on SiO_2 with CH_2Cl_2, then EtOAc, then CH_2Cl_2/MeOH (10 : 1) to give the product as a yellow solid.

***N*-[3-(4-{(*E*)-[4-(Octyloxy)phenyl]diazenyl}phenoxy)propyl]tetramethylguanidinium chloride (6a·Cl).** Yellow solid (39 mg, 75 μmol, 34%). FT-IR (ATR): $\tilde{\nu}$/cm^{-1} 2920s, 2851s, 1693m, 1597vs, 1578vs, 1500s, 1469m, 1403m, 1294w, 1236vs, 1169w, 1146s, 1105m, 1123m, 946w, 926w, 907w, 840s, 802m, 726s, 640w, 549m. ^{1}H-NMR (500 MHz, $CDCl_3$): δ = 0.89 (t, J = 6.9 Hz, 3H, CH_3), 1.25–1.38 (m, 8H, CH_2), 1.45–1.49 (m, 2H, CH_2), 1.78–1.85 (m, 2H, CH_2), 2.35–2.40 (m, 2H, $OCH_2CH_2CH_2N$), 2.92 (br s, 6H, $N[CH_3]_2$), 3.08 (br s, 6H, $N[CH_3]_2$), 3.47–3.50 (m, 2H, NCH_2), 4.03 (t, J = 6.3, 2H, OCH_2), 4.16 (t, J = 5.7, 2H, 1″-H), 6.95–7.00 (m, 4H, 3,3′-H), 7.85–7.87 (m, 4H, 2,2′-H), 9.76 (br t, 1H, N–H) ppm. ^{13}C-NMR (125 MHz, $CDCl_3$): δ = 14.1 (CH_3), 22.7, 26.0, 28.9, 29.2, 29.2, 29.4, 31.8 (CH_2), 40.0 ($N[CH_3]_2$), 40.5 ($N[CH_3]_2$), 42.4 (C–N), 65.0 (C-1″), 68.4 (C–O), 114.5 (C-3′), 114.7 (C-3), 124.4 (C-2′), 124.4 (C-2), 146.8 (C-1′), 147.3 (C-1), 160.4 (C═N), 161.4 (C-4′), 161.8 (C-4) ppm. MS (ESI): m/z 482.35 $[M]^+$. HRMS (ESI): calcd for $[C_{28}H_{44}N_5O_2]^+$ 482.3490, found 482.3490 $[M]^+$.

***N*-[4-(4-{(*E*)-[4-(Octyloxy)phenyl]diazenyl}phenoxy)butyl]tetramethylguanidinium chloride (6b·Cl).** Yellow solid (204 mg, 380 μmol, 65%). FT-IR (ATR): $\tilde{\nu}$/cm^{-1} 2921s, 2852s, 1599s, 1578vs, 1500m, 1472m, 1401m, 1316m, 1241vs, 1171w, 1146s, 1105w, 1065w, 1025m, 1002m, 895w, 841s, 776w, 759w, 728w, 641w, 551s. ^{1}H-NMR (250 MHz, $CDCl_3$): δ = 0.89 (t, J = 6.8 Hz, 3H, CH_3), 1.30–1.50 (m, 10H, CH_2), 1.76–2.05 (m, 6H, CH_2), 2.94 (br s, 6H, $N[CH_3]_2$), 3.10 (br s, 6H, $N[CH_3]_2$), 3.27–3.35 (m, 2H, NCH_2), 4.00–4.10 (m, 4H, 1″-H, OCH_2), 6.94–7.00 (m, 4H, 3,3′-H), 7.84–7.87 (m, 4H, 2,2′-H), 9.69 (br t, 1H, N–H) ppm. ^{13}C-NMR (125 MHz, $CDCl_3$): δ = 14.1 (CH_3), 22.7, 26.0, 26.5, 26.6,

29.2, 29.2, 29.4, 31.8 (CH_2), 40.0 ($N[CH_3]_2$), 40.6 ($N[CH_3]_2$), 45.2 (C–N), 67.6 (C-1″), 68.3 (C–O), 114.6 (C-3′), 114.7 (C-3), 124.3 (C-2′), 124.3 (C-2), 146.8 (C-1′), 147.0 (C-1), 160.7 (C═N), 161.3 (C-4′), 161.4 (C-4) ppm. MS (ESI): *m*/*z* 496.36 $[M]^+$. HRMS (ESI): calcd for $[C_{29}H_{46}N_5O_2]^+$ 496.3646, found 496.3631 $[M]^+$.

***N*-[5-(4-{(*E*)-[4-(Octyloxy)phenyl]diazenyl}phenoxy)pentyl]tetramethylguanidinium chloride (6c·Cl).** Yellow solid (50 mg, 92 μmol, 21%). FT-IR (ATR): $\tilde{\nu}$/cm^{-1} 2925s, 2851s, 1621s, 1598s, 1578vs, 1498s, 1469s, 1406m, 1317w, 1238vs, 1167w, 1142s, 1105w, 1072w, 1044w, 1000m, 924w, 898w, 835s, 809w, 776w, 725m, 640w, 547s. ^{1}H-NMR (250 MHz, $CDCl_3$): δ = 0.89 (t, *J* = 6.8 Hz, 3H, CH_3), 1.29–1.60 (m, 12H, CH_2), 1.76–1.94 (m, 6H, CH_2), 2.92 (br s, 6H, $N[CH_3]_2$), 3.11 (br s, 6H, $N[CH_3]_2$), 3.19–3.28 (m, 2H, NCH_2), 4.00–4.06 (m, 4H, 1″-H, OCH_2), 6.95–7.00 (m, 4H, 3,3′-H), 7.84–7.87 (m, 4H, 2,2′-H), 9.77 (br t, 1H, N–H) ppm. ^{13}C-NMR (125 MHz, $CDCl_3$): δ = 14.1 (CH_3), 22.7, 23.5, 26.0, 28.7, 29.2, 29.2, 29.4, 29.4, 31.8 (CH_2), 39.9 ($N[CH_3]_2$), 40.6 ($N[CH_3]_2$), 45.4 (C–N), 67.8 (C-1″), 68.3 (C–O), 114.6 (C-3′), 114.7 (C-3), 124.3 (C-2,2′), 146.9 (C-1′), 147.0 (C-1), 160.9 (C═N), 161.2 (C-4′), 161.4 (C-4) ppm. MS (ESI): *m*/*z* 510.38 $[M]^+$. HRMS (ESI): calcd for $[C_{30}H_{48}N_5O_2]^+$ 510.3803, found 510.3767 $[M]^+$.

***N*-[6-(4-{(*E*)-[4-(Octyloxy)phenyl]diazenyl}phenoxy)hexyl]tetramethylguanidinium chloride (6d·Cl).** Yellow solid (396 mg, 710 μmol, 68%). FT-IR (ATR): $\tilde{\nu}$/cm^{-1} 2931s, 2853s, 1620s, 1599vs, 1578vs, 1495m, 1469m, 1405w, 1316m, 1296w, 1238vs, 1185w, 1147s, 1106w, 1071w, 1044w, 1023w, 995w, 944w, 899w, 847s, 835s, 814w, 779w, 762w, 731w, 639w, 553s. ^{1}H-NMR (250 MHz, $CDCl_3$): δ = 0.89 (t, *J* = 6.8 Hz, 3H, CH_3), 1.30–1.59 (m, 12H, CH_2), 1.77–1.94 (m, 8H, CH_2), 2.93 (br s, 6H, $N[CH_3]_2$), 3.10 (br s, 6H, $N[CH_3]_2$), 3.17–3.25 (m, 2H, NCH_2), 4.00–4.05 (m, 4H, 1″-H, OCH_2), 6.95–7.00 (m, 4H, 3,3′-H), 7.84–7.87 (m, 4H, 2,2′-H), 9.80 (br t, 1H, N–H) ppm. ^{13}C-NMR (125 MHz, $CDCl_3$): δ = 14.1 (CH_3), 22.7, 25.6, 26.0, 26.6, 29.0, 29.2, 29.2, 29.4 29.7, 31.8 (CH_2), 39.9 ($N[CH_3]_2$), 40.6 ($N[CH_3]_2$), 45.4 (C–N), 68.0 (C-1″), 68.3 (C–O), 114.6 (C-3′), 114.7 (C-3), 124.3 (C-2′,2), 146.8 (C-1′), 146.9 (C-1), 161.0 (C═N), 161.2 (C-4′), 161.4 (C-4) ppm. MS (ESI): *m*/*z* 524.40 $[M]^+$. HRMS (ESI): calcd for $[C_{31}H_{50}N_5O_2]^+$ 524.3959, found 524.3967 $[M]^+$.

***N*-[7-(4-{(*E*)-[4-(Octyloxy)phenyl]diazenyl}phenoxy)heptyl]tetramethylguanidinium chloride (6e·Cl).** Yellow solid (149 mg, 260 μmol, 72%). FT-IR (ATR): $\tilde{\nu}$/cm^{-1} 2932s, 2853s, 1599vs, 1579vs, 1497m, 1471m, 1402m, 1316m, 1296w, 1244vs, 1446s, 1105w, 1069w, 1026m, 946w, 898w, 842s, 777w, 727w, 640w, 604w, 552s. ^{1}H-NMR (250 MHz, $CDCl_3$): δ = 0.89 (t, *J* = 6.8 Hz, 3H, CH_3), 1.29–1.47 (m, 16H, CH_2), 1.72–1.87 (m, 6H, CH_2), 2.93 (br s, 6H, $N[CH_3]_2$), 3.10 (br s, 6H, $N[CH_3]_2$), 3.16–3.24 (m, 2H, NCH_2), 4.00–4.05 (m, 4H, 1″-H, OCH_2), 6.96–7.00 (m, 4H, 3,3′-H), 7.84–7.87 (m, 4H, 2,2′-H), 9.38 (br t, 1H, N–H) ppm. ^{13}C-NMR (125 MHz, $CDCl_3$): δ = 14.1 (CH_3), 22.7, 25.9, 26.0, 26.9, 28.9, 29.0, 29.2, 29.2, 29.4, 29.7, 31.8 (CH_2), 39.9 ($N[CH_3]_2$), 40.6 ($N[CH_3]_2$), 45.5 (C–N), 68.1 (C-1″), 68.3 (C–O), 114.7 (C-3′,3), 124.3 (C-2′,2), 146.9 (C-1′), 146.9 (C-1), 161.1 (C═N), 161.2 (C-4′), 161.5 (C-4) ppm. MS (ESI): *m*/*z* 538.41 $[M]^+$. HRMS (ESI): calcd for $[C_{32}H_{52}N_5O_2]^+$ 538.4116, found 538.4109 $[M]^+$.

***N*-[8-(4-{(*E*)-[4-(Octyloxy)phenyl]diazenyl}phenoxy)octyl]tetramethylguanidinium chloride (6f·Cl).** Yellow solid (0.40 g, 68%). FT-IR (ATR): $\tilde{\nu}$/cm^{-1} 2920s, 2852s, 1600vs, 1579vs, 1497m, 1472m, 1403m, 1316m, 1296w, 1242vs, 1179w, 1147s, 1107m, 1167w, 1123m, 1001m, 943w, 898w, 843vs, 776w, 727w, 640w, 554s. ^{1}H-NMR (250 MHz, $CDCl_3$): δ = 0.89 (t, *J* = 6.8 Hz, 3H, CH_3), 1.30–1.47 (m, 18H, CH_2), 1.78–1.84 (m, 6H, CH_2), 2.92 (br s, 6H, $N[CH_3]_2$), 3.10 (br s, 6H, $N[CH_3]_2$), 3.15–3.23 (m, 2H, NCH_2), 4.00–4.05 (m, 4H, 1″-H, OCH_2), 6.96–7.00 (m, 4H, 3,3′-H), 7.84–7.87 (m, 4H, 2,2′-H), 9.76 (br t, 1H, N–H) ppm. ^{13}C-NMR (125 MHz, $CDCl_3$): δ = 14.1 (CH_3), 22.7, 25.9, 26.0, 26.9, 29.1, 29.1, 29.2, 29.2, 29.4, 29.8, 31.8 (CH_2), 39.9 ($N[CH_3]_2$), 40.6 ($N[CH_3]_2$), 45.5 (C–N), 68.2 (C-1″), 68.3 (C–O), 114.7 (C-3′,3), 124.3 (C-2′,2), 146.9 (C-1′), 146.9 (C-1), 161.1 (C═N), 161.2 (C-4′), 161.5 (C-4) ppm. MS (ESI): *m*/*z* 552.43 $[M]^+$. HRMS (ESI): calcd for $[C_{33}H_{54}N_5O_2]^+$ 552.4272, found 552.4260 $[M]^+$.

Crystal structure determination of guanidinium bromide 6b·Br (CCDC 1030119).

Crystal data. $C_{29}H_{48}BrN_5O_3$, *M* = 594.63, triclinic, *a* = 8.0979(1), *b* = 10.1206(6), *c* = 20.3102(12) Å, *V* = 1526.23(15) Å^3, *T* = 100 K, space group $P\bar{1}$, *Z* = 2, 26 683 reflections measured, 7547 unique (R_{int} = 0.0443) which were used in all calculations. The final w$R(F_2)$ was 0.0911 (all data).

Acknowledgements

Financial support by the Deutsche Forschungsgemeinschaft (grant # La 907/17-1, Gi 243/8-1), the Bundesministerium für Bildung und Forschung (shared instrumentation grant # 01 RI 05177), the Ministerium für Wissenschaft, Forschung und Kunst des Landes Baden-Württemberg, the Forschungsfonds der Universität Stuttgart and the Fonds der Chemischen Industrie is gratefully acknowledged.

References

1 (*a*) G. Pelzl, *Z. Chem.*, 1977, **17**, 294–295; (*b*) C. Leier and G. Pelzl, *J. Prakt. Chem.*, 1979, **321**, 197–204.
2 K. F. Nelson, W. E. Haas and J. E. Adams, *J. Electrochem. Soc.*, 1975, **122**, 1564–1565.
3 (*a*) S. Kurihara, T. Ikeda and S. Tazuke, *Mol. Cryst. Liq. Cryst.*, 1990, **178**, 117–132; (*b*) S. Tazuke, S. Kurihara and T. Ikeda, *Chem. Lett.*, 1987, 911–914.
4 Reviews: (*a*) C. V. Yelamaggad, S. K. Prasad and Q. Li, *Liq. Cryst. Beyond Disp.*, 2012, 157–211; (*b*) S. K. Prasad, *Mol. Cryst. Liq. Cryst.*, 2009, **509**, 1059–1069; (*c*) R. P. Lemieux, *Soft Matter*, 2005, **1**, 348–354; (*d*) T. Ikeda, *J. Mater. Chem.*, 2003, **13**, 2037–2057; (*e*) F. Simoni and O. Francescangeli, *J. Phys.: Condens. Matter*, 1999, **11**, R439–R487.
5 Review: H. Yu, *J. Mater. Chem. C*, 2014, **2**, 3047–3054.
6 For previous studies on polymeric and dendritic azobenzene ILCs see: (*a*) T. Yoshimi, M. Moriyama and S. Ujiie, *Mol. Cryst. Liq. Cryst.*, 2009, **511**, 319–326; (*b*) Q. Zhang, X. Wang, C. J. Barrett and C. G. Bazuin, *Chem. Mater.*, 2009, **21**, 3216–3227; (*c*) S. Xiao, X. Lu, Q. Lu and B. Su, *Macromolecules*, 2008, **41**, 3884–3892; (*d*) M. Marcos, R. Alcala, J. Barbera, P. Romero, C. Sanchez and J. L. Serrano, *Chem. Mater.*, 2008,

20, 5209–5217; (*e*) S. Xiao, X. Lu and Q. Lu, *Macromolecules*, 2007, **40**, 7944–7950.

7 Q. Zhang, K. Wang, Q. Reu, L. Niu and B. Chen, *Liq. Cryst.*, 2011, **38**, 1349–1355.

8 Q. Zhang, C. Shan, X. Wang, L. Chen, L. Niu and B. Chen, *Liq. Cryst.*, 2008, **35**, 1299–1305.

9 (*a*) B. Ringstrand, H. Monobe and P. Kaszynski, *J. Mater. Chem.*, 2009, **19**, 4805–4812; (*b*) B. Ringstrand, A. Jankowiak, L. E. Johnson, P. Kaszynski, D. Pociecha and E. Gorecka, *J. Mater. Chem.*, 2012, **22**, 4874–4880.

10 S. Zhang, S. Liu, Y. Zhang and Y. Deng, *Chem. – Asian J.*, 2012, **7**, 2004–2007.

11 Reviews on ILCs: (*a*) M. Mansueto and S. Laschat, in *Handbook of Liquid Crystals*, ed. J. W. Goodby, P. J. Collings, T. Kato, C. Tschierske, H. F. Gleeson and R. Raynes, Wiley-VCH, Weinheim, 2nd edn, 2014, ch. 8, vol. 6, pp. 231–280; (*b*) B. Ringstrand and P. Kaszynski, *Acc. Chem. Res.*, 2013, **46**, 214–225; (*c*) K. V. Axenov and S. Laschat, *Materials*, 2011, **4**, 206–259; (*d*) K. Binnemans, *Chem. Rev.*, 2005, **105**, 4148–4204.

12 P. Beyer, M. Krueger, F. Giesselmann and R. Zentel, *Adv. Funct. Mater.*, 2007, **17**, 109–114.

13 (*a*) J. Garcia-Amorós, H. Finkelmann and D. Velasco, *Phys. Chem. Chem. Phys.*, 2011, **13**, 11233–11238; (*b*) J. Garcia-Amorós, H. Finkelmann and D. Velasco, *Chem. – Eur. J.*, 2011, **17**, 6518–6523.

14 H. G. Walton, H. J. Coles, D. Guillon and G. Poeti, *Liq. Cryst.*, 1994, **17**, 333–349.

15 Z. Shi, H. Lu, Z. Chen, R. Cheng and D. Cheng, *Polymer*, 2012, **53**, 359–369.

16 K. Kanie and T. Sugimoto, *J. Am. Chem. Soc.*, 2003, **125**, 10518–10519.

17 S. Sauer, N. Steinke, A. Baro, S. Laschat, F. Giesselmann and W. Kantlehner, *Chem. Mater.*, 2008, **20**, 1909–1915.

18 (*a*) S. Sauer, S. Saliba, S. Tussetschläger, A. Baro, W. Frey, F. Giesselmann, S. Laschat and W. Kantlehner, *Liq. Cryst.*, 2009, **36**, 275–299; (*b*) M. Butschies, S. Sauer, E. Kessler, H.-U. Siehl, B. Claasen, P. Fischer, W. Frey and S. Laschat, *ChemPhysChem*, 2010, **11**, 3752–3765.

19 N. Kapernaum and F. Giesselmann, *Phys. Rev. E: Stat., Nonlinear, Soft Matter Phys.*, 2008, **78**, 062701.

20 (*a*) Y. Takanishi, A. Ikeda, H. Takezoe and A. Fukuda, *Phys. Rev. E: Stat. Phys., Plasmas, Fluids, Relat. Interdiscip. Top.*, 1995, **51**, 400–406; (*b*) E. F. Gramsbergen and W. H. De Jeu, *Liq. Cryst.*, 1989, **4**, 449–455; (*c*) J. Watanabe and M. Hayashi, *Macromolecules*, 1989, **22**, 4083–4088.

21 P. Davidson, D. Petermann and A. M. Levelut, *J. Phys. II*, 1995, **5**, 113–131.

22 (*a*) W. L. McMillan, *Phys. Rev. A: At., Mol., Opt. Phys.*, 1972, **6**, 936–947; (*b*) A. J. Leadbetter and E. K. Norris, *Mol. Phys.*, 1979, **38**, 669–686; (*c*) W. Haase, Z. X. Fan and H. J. Mueller, *J. Chem. Phys.*, 1988, **89**, 3317–3322; (*d*) A. Sanchez-Castillo, M. A. Osipov, S. Jagiella, Z. H. Nguyen, M. Kaspar, V. Hamplova, J. Maclennan and F. Giesselmann, *Phys. Rev. E: Stat., Nonlinear, Soft Matter Phys.*, 2012, **85**, 061703.

23 S. T. Lagerwall, P. Rudquist and F. Giesselmann, *Mol. Cryst. Liq. Cryst.*, 2009, **510**, 148–157.

24 S. Diele, *Ber. Bunsen-Ges. Phys. Chem.*, 1993, **97**, 1326–1336.

25 (*a*) G. Casella, V. Causin, F. Rastrelli and G. Saielli, *Phys. Chem. Chem. Phys.*, 2014, **16**, 5048–5051; (*b*) V. Causin and G. Saielli, *J. Mater. Chem.*, 2009, **19**, 9153–9162.

26 (*a*) C. M. Gordon, J. D. Holbrey, A. R. Kennedy and K. R. Seddon, *J. Mater. Chem.*, 1998, **8**, 2627–2636; (*b*) J. Dupont, C. S. Consorti, P. A. Z. Suarez and R. F. de Souza, *Org. Synth.*, 2002, **79**, 236–243; (*c*) T. Inoue, B. Dong and L.-Q. Zheng, *J. Colloid Interface Sci.*, 2007, **307**, 578–581.

27 M. Ito, T. X. Wei, P.-L. Chen, H. Akiyama, M. Matsumoto, K. Tamada and Y. Yamamoto, *J. Mater. Chem.*, 2005, **15**, 478–483.

28 D. Rais, Y. Zakrevskyy, J. Stumpe, S. Nespůrek and Z. Sedláková, *Opt. Mater.*, 2008, **30**, 1335–1342.